Gold-decorated TiO_2 nanofibrous hybrid for improved solar-driven photocatalytic pollutant degradation

Karen Yuanting Tang,[a#] James Xiaoyuan Chen,[a#] Enrico Daniel R. Legaspi,[b#] Cally Owh,[a] Ming Lin,[a] Ice Si Yin Tee,[a] Dan Kai,[a] Xian Jun Loh,[a] Zibiao Li,[a] Michelle D. Regulacio[c,d]* and Enyi Ye[a]**

[a] Institute of Materials Research and Engineering, Agency for Science, Technology and Research (A*STAR), 2 Fusionopolis Way, 138634 Singapore

[b] Materials Science and Engineering Program, University of the Philippines Diliman, Quezon City, 1101, Philippines

[c] Institute of Chemistry, University of the Philippines Diliman, Quezon City, 1101, Philippines

[d] National Sciences Research Institute (NSRI), University of the Philippines Diliman, Quezon City, 1101 Philippines

[#]These authors contributed equally

*corresponding authors

E-mail: lizb@imre.a-star.edu.sg; mdregulacio@up.edu.ph; yeey@imre.a-star.edu.sg

Keywords: titanium dioxide, gold, nanocomposite, nanofiber, electrospinning, photocatalyst, dye degradation

Highlights

- Facile fabrication of gold nanoparticles decorated TiO_2 nanofibrous hybrid photocatalyst
- Highly efficient solar-driven photocatalytic pollutant degradation
- Dual functions of gold nanoparticles for effective charge separation and plasmon enhanced solar light photocatalysis
- Successful demonstration of effective solar-driven photocatalytic degradation of Rhodamine B (RhB) and methyl blue (MB).

Gold-decorated TiO_2 nanofibrous hybrid for improved solar-driven photocatalytic pollutant degradation

Karen Yuanting Tang,[a#] *James Xiaoyuan Chen,*[a#] *Enrico Daniel R. Legaspi,* [b#] *Cally Owh,*[a] *Ming Lin,*[a] *Ice Si Yin Tee,*[a] *Dan Kai,*[a] *Xian Jun Loh,*[a] *Zibiao Li,*[a]* *Michelle D. Regulacio* [c,d]* *and Enyi Ye* [a]*

[a] Institute of Materials Research and Engineering, Agency for Science, Technology and Research (A*STAR), 2 Fusionopolis Way, 138634 Singapore

[b] Materials Science and Engineering Program, University of the Philippines Diliman, Quezon City, 1101, Philippines

[c] Institute of Chemistry, University of the Philippines Diliman, Quezon City, 1101, Philippines

[d] National Sciences Research Institute (NSRI), University of the Philippines Diliman, Quezon City, 1101 Philippines

[#]These authors contributed equally

*corresponding authors

E-mail: lizb@imre.a-star.edu.sg; mdregulacio@up.edu.ph; yeey@imre.a-star.edu.sg

Keywords: titanium dioxide, gold, nanocomposite, nanofiber, electrospinning, photocatalyst, dye degradation

Abstract

TiO_2-based nanomaterials are among the most promising photocatalysts for degrading organic dye pollutants. In this work, Au–TiO_2 nanofibers were fabricated by the electrospinning technique, followed by calcination in air at 500 °C. Morphological and structural analyses revealed that the composite consists of TiO_2 nanofibers with embedded Au nanoparticles that are extensively distributed throughout the porous fibrous structure of TiO_2. The photocatalytic performance of these Au-embedded TiO_2 nanofibers was evaluated in the photodegradation of Rhodamine B and methylene blue under solar simulator irradiation. Compared with pristine TiO_2 nanofibers, the Au-embedded TiO_2 nanofibers displayed far better photocatalytic degradation efficiency. The plasmon resonance absorption of Au nanoparticles in the visible spectral region and the effective charge separation at the heterojunction of the Au–TiO_2 hybrid are the key factors that have led to the considerable enhancement of the photocatalytic activity. The results of this study clearly demonstrate the potential of Au–TiO_2 electrospun nanofibers as solar-light-responsive photocatalysts for the effective removal of dye contaminants from aquatic environments.

1. Introduction

With the onset of the 21st century, the globalization of industries has led to an unprecedented increase in the manufacturing of both consumer goods and industrial products. This massive scale of production comes with the unavoidable drawback of a proportionally large amount of industrial waste. Of the many concerns brought about by these waste products, wastewater pollution caused by chemical factories and manufacturing plants is one of the most immediate ones. A large group of pollutants that is responsible for wastewater contamination consists of organic dyes, which are widely used in the manufacturing of textiles, cosmetics, paper, and leather, and can consequently be found in the effluent of these industries (He et al., 2018; Berradi et al., 2019). It has been estimated that 15% of the dyes used in these manufacturing processes are released into different bodies of water. Because these compounds are non-biodegradable, they can remain in water systems for extended amounts of time, adversely affecting the aquatic ecosystems as well as humans who rely on these bodies of water for sustenance. Moreover, due to biomagnification, larger concentrations of these dyes are found in the wildlife commonly consumed by humans (Lellis et al., 2019).

To tackle the presence of hazardous organic dyes in our water systems, various physical and chemical treatment processes have been developed. One such process is the use of photocatalysts to degrade these organic dyes. In photocatalysis, a light-harvesting material is used to promote the decomposition of organic pollutants into less harmful intermediates in the presence of light. Metal oxide semiconductors such as TiO_2, ZnO, and SnO_2 have been the main focus of photocatalyst-based wastewater treatment as they have been shown to exhibit notable photocatalytic efficiency (Hoffmann et al., 1995; Chan et al., 2011; Al-Hamdi et al., 2017; Thuong et al., 2019). A typical photocatalytic process begins with the absorption of photons with energy greater than the band

gap of the semiconductor. Electrons in the valence band are promoted to the conduction band and leave behind a hole, forming an exciton pair. Exciton pairs can either migrate to the surface of the material or recombine (Ma et al., 2014). The photogenerated electrons and holes that successfully reach the surface can generate free radicals that interact with organic dye pollutants in redox reactions and break them down into more environmentally favorable intermediates (Ajmal et al., 2014). The photocatalytic activity for dye degradation is thus largely determined by the ability of the semiconductor to strongly absorb light and create electron–hole pairs that can drive the dye decomposition reactions.

Of all the semiconductors that are used as photocatalysts, nanosized TiO_2 is the most extensively studied owing to its low toxicity, chemical and thermal stability, resistance to photocorrosion, cheap cost, and widespread availability (Al-Mamun et al., 2019; Gopinath et al., 2020). Both the anatase and rutile forms of TiO_2 have been shown capable of degrading organic dyes, such as methylene blue, methyl orange, Rhodamine B, indigo carmine, and Eriochrome Black T, under ultraviolet (UV) irradiation (Gautam et al., 2016; Kochkina et al., 2017). However, a significant drawback seen in these studies is the fact that a UV light source must be used to induce the photocatalytic process due to the wide band gap of TiO_2 (E_g = 3.2 eV for anatase, 3.0 eV for rutile) (Khalid et al., 2017). This can severely limit its application for large-scale industrial use. As a response to this concern, researchers have studied the modification of TiO_2 by creating a hybrid with a photosensitizer that allows for absorption of visible light (Djurišić et al., 2014). This would allow for photocatalysis under solar light, which is strongly favorable for industrial and commercial use. Another limitation of TiO_2 is its fast recombination rate, which is detrimental to photocatalysis as less photogenerated charge carriers become available to participate in the dye degradation process (Nam et al., 2019). The pairing of TiO_2 with plasmonic Au nanoparticles is a

promising remediation to the disadvantages of pristine TiO_2. Au nanoparticles exhibit a phenomenon called localized surface plasmon resonance (LSPR), which can boost the photocatalytic performance through energy transfer mechanisms that can enhance the charge carrier concentration in TiO_2 (Linic et al., 2011). As the LSPR of Au nanoparticles lies in the visible spectral range, coupling TiO_2 with Au nanoparticles enables absorption of visible photons, which constitute a large portion of the solar spectrum. In addition, Au has been found to inhibit electron–hole recombination by separating photogenerated electron–hole pairs and promoting interfacial charge transfer (Bumajdad et al., 2014).

The synthesis of Au–TiO_2 nanocomposites is typically done in solution. One of the most common protocols is the deposition–precipitation method, where Au nanoparticles are randomly deposited onto the surface of pre-synthesized TiO_2 nanoparticles (Amrollahi et al., 2014; Bumajdad et al., 2014). However, the nanoparticles that are prepared through this approach have a tendency to flocculate in solution, which may negatively affect their photocatalytic activity and limit their reusability. Another technique is to allow TiO_2 to anisotropically grow onto pre-synthesized Au nanostructures in the presence of surfactants. A variety of hybrid configurations, such as Janus, core–shell, and flower-like architectures, have been produced through this strategy (Li and Zeng, 2005; Seh et al., 2011). The foremost challenge faced by solution-phase methods is that they are limited to small-scale production. A commercially viable way of producing Au–TiO_2 hybrid nanostructures is through the polymer-assisted electrospinning process. Electrospinning is an economical and scalable method for fabricating one-dimensional (1D) nanomaterials with inherent porosity. For instance, electrospun TiO_2 with mesoporous 1D fiber-like structures have been successfully prepared through this approach (Li and Xia, 2003; Cossich et al., 2015; Someswararao et al., 2018; Roongraung et al., 2020). The general setup involves loading a syringe

with the precursor solution and connecting its conductive needle tip to a high voltage power supply (Soo et al., 2019). The solution is subsequently ejected out of the needle by a syringe pump into a stable jet, which is elongated by the electric current to form a continuous thin fiber (Ligon et al., 2018). Several copies of the resultant fiber can be formed in a short amount of time under the continuous-feeding mode. These nanofibers are then deposited onto the surface of a grounded collector, and are later subjected to calcination in air. To create Au–TiO_2 electrospun nanofibers, pre-synthesized Au nanoparticles are included in the precursor solution prior to the electrospinning process (Duan et al., 2019; Kumar et al., 2020). The resulting hybrid consists of TiO_2 nanofibers that are sparsely decorated with Au nanoparticles.

In this study, Au–TiO_2 electrospun nanofibers have been synthesized through a more facile procedure that does not require the pre-synthesis of Au nanoparticles. Analysis of the morphological structure of the calcined sample revealed that our protocol produced porous polycrystalline TiO_2 nanofibers with embedded Au nanoparticles that are extensively distributed throughout the fibrous structure. The photocatalytic performance of the Au–TiO_2 composite nanofibers was compared against that of pristine TiO_2 nanofibers under solar irradiation for dye pollutant degradation using Rhodamine B (RhB) and methylene blue (MB) dyes. Our results indicate that the embedded Au nanoparticles can effectively enhance the photocatalytic activity of TiO_2.

2. Experimental Section

2.1 Synthesis of Au–TiO_2 nanofibers

In a typical procedure, 0.32 mL titanium tetraisopropoxide (TTIP) was mixed with 0.6 mL ethanol and 0.6 mL acetic acid in a glovebox. The resultant pale-yellow solution was then added

to 1.5 mL ethanol with 0.18 g polyvinylpyrrolidone (PVP, MW = 1,300,000) and 15 mg $AuCl_3$. The mixture was stirred vigorously for ~1 hr to form a homogeneous solution, which was then loaded into a 6-mL syringe with a blunt 22-gauge needle (inner diameter of 0.413 mm). The brownish solution was spun at a constant rate of 0.8 mL/h with a voltage of 12 kV applied to the needle. The nanofibers were collected on an aluminum foil (collector) with a distance of 20 cm from the needle. The obtained nanofibers were left in ambient conditions overnight to allow for full hydrolysis of TTIP. This was followed by calcination at 500 °C in air for 3 h to remove PVP and other carbonaceous materials. The color of the nanofibers turned from white (before calcination) to bluish violet (after calcination). Pristine TiO_2 nanofibers were also prepared using the same procedure but without adding $AuCl_3$ into the precursor solution. In this case, the nanofibers remained white even after calcination.

2.2 Characterization of Au–TiO_2 nanofibers

The X-ray diffraction (XRD) patterns of the Au–TiO_2 nanofibers (before and after the calcination step) and the pristine TiO_2 nanofibers were measured using a Bruker GADDS D8 Discover diffractometer with Cu_{Ka} radiation at a working voltage and current of 40 kV and 40 mA, respectively. In preparing the samples, the nanofibers were placed on a 1×1 cm^2 silicon wafer. The morphology of the nanofibers was characterized using a JEOL JSM 6700F field emission scanning electron microscope (FESEM) in transmission mode. The samples were coated with a thin layer of platinum via sputtering prior to imaging. The morphology of the nanofibers was further analyzed using a FEI Titan transmission electron microscope (TEM). Bright-field TEM images were collected at an accelerating voltage of 200 kV. High-angle annular dark-field scanning TEM (HAADF-STEM) images of the Au–TiO_2 nanofibers were also acquired using the

STEM mode. Energy dispersive X-ray (EDX) elemental mapping was performed to obtain the Au, Ti and O elemental maps. For the UV-Vis absorption measurements, the nanofibers were dispersed in deionized water under sonication for 2 min prior to analysis. The absorption spectra were recorded at room temperature using a Shimadzu UV-1800 spectrophotometer.

2.3 Photocatalytic Dye Degradation Study

The photocatalytic performance of the Au–TiO_2 nanofibers was evaluated in the photocatalytic degradation of RhB (Rhodamine B, Sigma-Aldrich, ≥ 95%) and MB (methylene blue, Sigma-Aldrich, ≥ 82%). In a typical experiment, 5 mg of the nanofibers were dispersed in a 50-mL aqueous solution of the dye (RhB or MB), and the resulting mixture was left to stir for 1 h in the dark to establish an adsorption–desorption equilibrium. The mixture was then irradiated using a solar simulator (AM 1.5G). At specified time intervals, a 1-ml aliquot of the mixture was periodically taken out and then centrifuged to remove the nanofiber photocatalyst. The absorption spectra of the supernatant were measured using a Shimadzu UV-1800 spectrophotometer to monitor the change in the dye concentration. For RhB, the change in concentration was monitored by measuring the absorbance at 553 nm. Meanwhile, the MB concentration was monitored by taking the absorbance at 668 nm. The extent of degradation over time was determined by calculating C/C_0, where C_0 and C are the absorbance of the dye solution before and after irradiation, respectively. For comparison purposes, the photocatalytic performance of the pristine TiO_2 nanofibers was also measured under the same experimental conditions.

3. Results and Discussion

3.1 Synthesis of Au–TiO_2 nanofibers

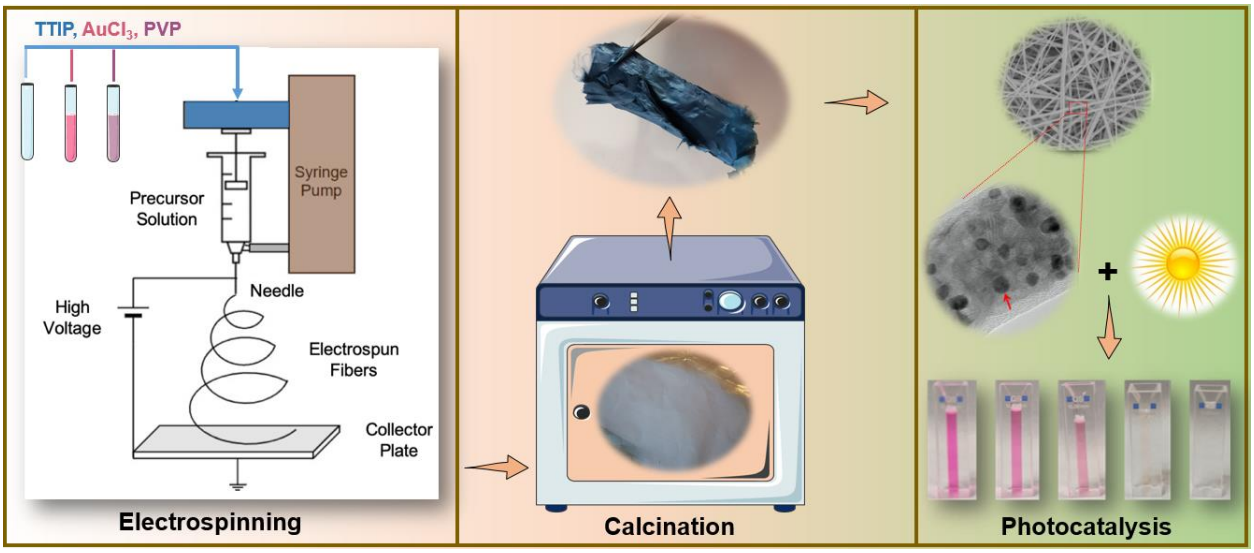

Fig. 1. Schematic illustration showing the fabrication of Au-decorated TiO_2 nanofibers and their use as a highly efficient photocatalyst for dye pollutant degradation under solar light.

Fig. 1 presents a schematic illustration of the experimental setup that was used in our fabrication of Au–TiO_2 nanofibers. The electrospinning process is shown in the first panel. In previously published electrospinning procedures for Au–TiO_2 nanofibers, colloidal Au nanoparticles are first prepared separately, and then a solution of these nanoparticles is mixed with the TiO_2 precursor solution prior to electrospinning (Duan et al., 2019; Kumar et al., 2020). By contrast, our synthetic approach does not make use of pre-synthesized Au nanoparticles. Instead, $AuCl_3$ (a precursor to Au) was directly mixed with the TiO_2 precursor solution, and the resultant solution is subsequently subjected to electrospinning. The elimination of the pre-synthesis step makes our procedure

simpler and less tedious. The TiO_2 precursor solution is an ethanolic solution that contains TTIP (a titanium alkoxide that serves as a precursor to TiO_2) and PVP, which is a polymer that assists in the formation of a fibrous morphology. The nanofibers that were obtained after the electrospinning process were left to stand under ambient conditions to allow for complete hydrolysis of TTIP by moisture in air. They are then subjected to calcination in air at 500 °C to selectively remove carbonaceous materials from the fibers and to promote crystallization of the desired materials. The red and blue plots in Fig. 2a are the experimental XRD patterns of the nanofibers before and after the calcination step, respectively. The lack of prominent diffraction peaks in the XRD pattern of the nanofibers obtained before calcination denotes the absence of crystalline materials in the pre-calcined sample. Meanwhile, the final product obtained after calcination exhibits distinct diffraction peaks that can be attributed to face-centered cubic Au (JCPDS 04–0784) and the tetragonal anatase phase of TiO_2 (JCPDS 84–1826). This implies that the ensuing thermal treatment facilitated the formation and crystallization of Au and TiO_2. For comparison, pristine TiO_2 nanofibers were also fabricated and the experimental XRD pattern obtained after calcination is presented as the black plot in Fig. 2a. In this case, only the diffraction peaks that can be ascribed to TiO_2 are observed. The fibrous structure of the pre-calcined electrospun sample is evident in the SEM image in Fig. 2b. This 1D fiber-like morphology was preserved even after calcination, as shown in the SEM image of the final Au–TiO_2 composite in Fig. 2c. EDX analysis (Fig. 2d) confirms the presence of Au in the calcined fibers.

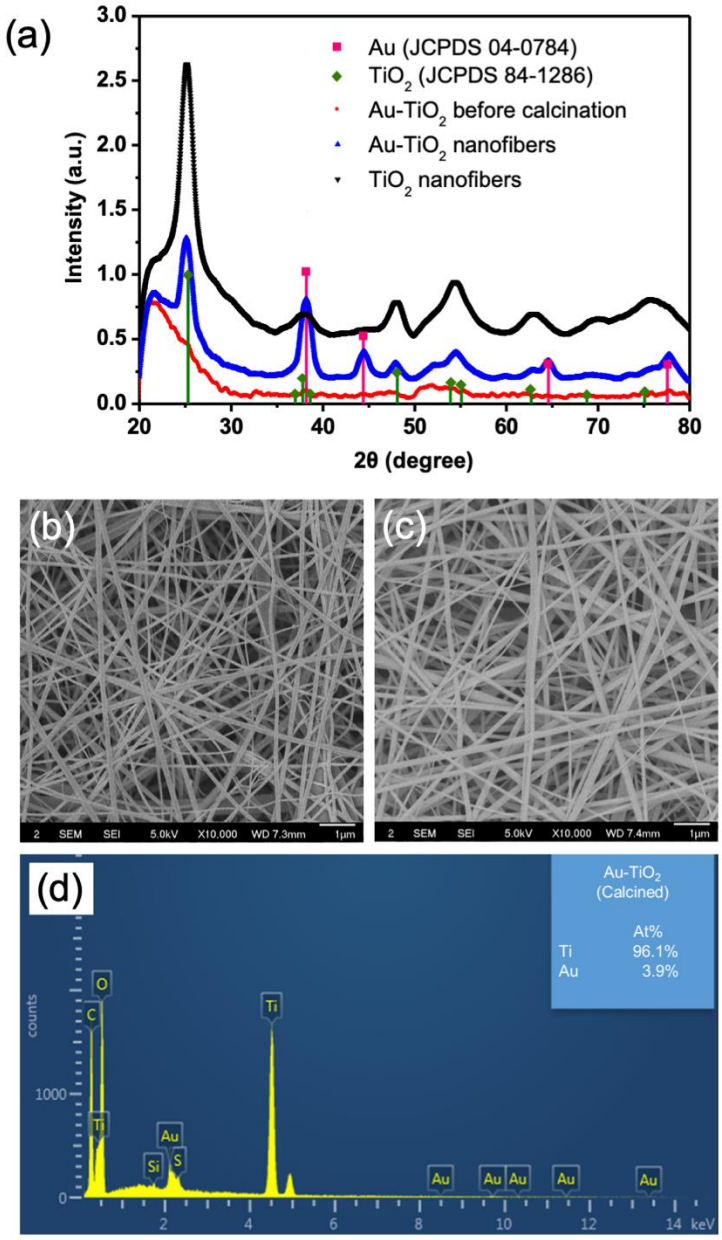

Fig. 2. (a) XRD patterns of the pristine TiO_2 nanofibers (black), Au–TiO_2 nanofibers (blue) and pre-calcined Au–TiO_2 nanofibers (red). The literature patterns for Au (pink) and anatase TiO_2 (green) are also shown. (b-c) SEM image of the Au–TiO_2 nanofibers (b) before and (c) after calcination. (d) EDX spectrum of the Au-TiO_2 nanofibers after calcination.

3.2 Morphological structure of Au–TiO_2 nanofibers

Size analysis of SEM images showed that the calcined Au–TiO_2 nanofibers have an average diameter of 143 ± 60 nm. As the Au nanoparticles are not visible in the SEM image, TEM imaging was used to further investigate the morphology and configuration of the composite nanofibers. Displayed in Fig. 3a-c are some representative TEM images of the Au–TiO_2 nanofibers. For comparison, the TEM images of the pristine TiO_2 nanofibers are also shown in Fig. 3d-f. From Fig. 3e, it can be observed that the pristine TiO_2 nanofibers have a very rough surface and are mesoporous. The high-resolution TEM image in Fig. 3f revealed multiple crystal domains, indicating that each nanofiber is composed of small TiO_2 crystallites that are randomly aggregated, and this accounts for the surface roughness and porosity of the fiber. For the Au–TiO_2 nanofibers, the TiO_2 fibrous structure retained its porous polycrystalline nature, while Au exists as tiny crystallites (average size: 5.5 ± 1.1 nm) that are entrapped within the porous fibers. The presence of embedded Au nanoparticles (darker contrast regions) is not very obvious in the low-resolution image (Fig. 3a) but becomes more noticeable with increasing magnification (Fig. 3b-c). It is worth noting that the Au nanoparticles in our Au–TiO_2 nanofibers are heavily and consistently distributed throughout the fibrous structure. This is different from the previously reported Au–TiO_2 electrospun nanofibers that were prepared using pre-synthesized colloidal Au nanoparticles, where the Au nanoparticles are only sparsely present in the resultant composite fibers (Duan et al., 2019; Kumar et al., 2020). Thus, an important advantage of our synthetic strategy is the extensive presence of embedded Au in our composite nanofibers as this is beneficial to the improvement of photocatalytic performance. It is likely that in our synthesis, Au^{3+} ions from $AuCl_3$ are entrapped within the nanofibers during the electrospinning process. In the succeeding calcination step, the

oxidation of carbonaceous materials becomes the driving force for the reduction of these Au^{3+} ions to Au nanoparticles.

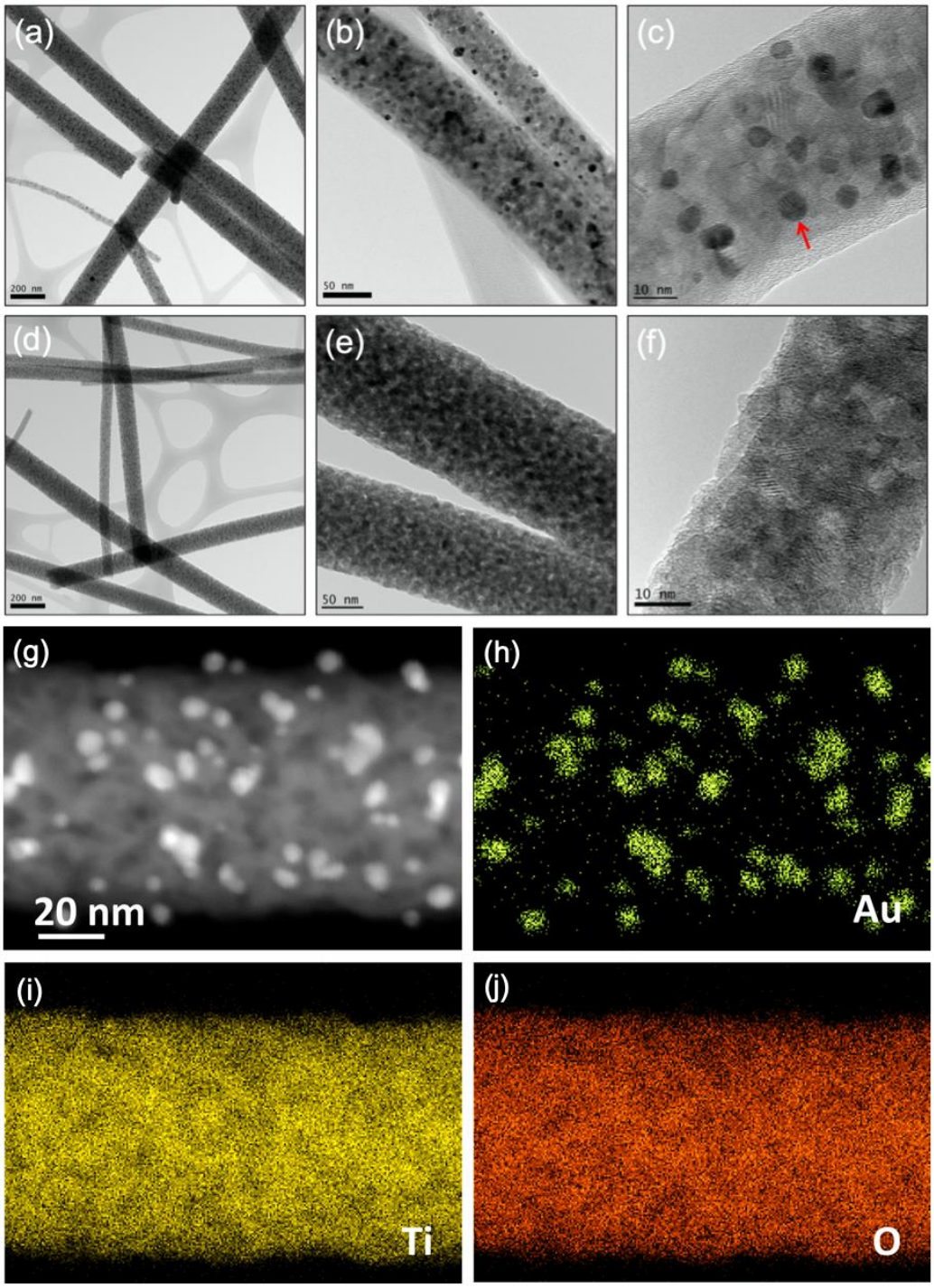

Fig. 3. TEM images of the (a-c) Au–TiO_2 nanofibers and (d-f) pristine TiO_2 nanofibers. The red arrow in (c) is used to highlight one of the embedded Au nanoparticles. (g) HAADF-STEM image of a representative Au-embedded TiO_2 nanofiber. Also shown are the EDX elemental maps for (h) Au, (i) Ti, and (j) O, corresponding to the image in (g).

High-angle annular dark-field scanning TEM (HAADF-STEM) was used to provide additional evidence that supports the existence of entrenched Au nanoparticles in our hybrid nanofibers. The Au nanoparticles can be clearly seen as bright regions in the HAADF-STEM image in Fig. 3g. Au is much brighter than TiO_2 in these images because of its higher atomic number relative to Ti and O. This is a consequence of the Z-contrast in HAADF-STEM. The corresponding EDX elemental maps were also taken to confirm the distribution of elements in the composite. The Au elemental map in Fig. 3h confirms that the bright regions in Fig. 3g are the embedded Au nanoparticles. Meanwhile, the elemental maps in Fig. 3i-j prove that the fibrous structure that hosts the Au nanoparticles is composed of Ti and O.

3.3 Photocatalytic properties of Au–TiO_2 nanofibers

The UV-Vis absorption spectra for the nanofibrous pristine TiO_2 (black plot) and Au–TiO_2 (blue plot) are displayed in Fig. 4. Both spectra show a distinct absorption band peaking at around 330 nm in the UV spectral region, which is characteristic of TiO_2. For the Au–TiO_2 nanofibers, there is also a broad absorption band with substantial intensity that appears in the visible spectral range, which accounts for the bluish-violet color of the hybrid. The center of the band is seen as a shoulder at around 570 nm and this is attributed to the LSPR-induced absorption of the embedded 5-nm Au nanoparticles. For comparison, Au nanoparticles of similar size were prepared and their

UV-Vis absorption spectrum was also measured (red plot in Fig. 4). These bare Au nanoparticles are red when dispersed in water, and exhibit a well-defined LSPR absorption band in the visible region. The band is centered at around 528 nm, which is typical for small-sized Au nanoparticles (Hu et al., 2006). The longer-wavelength visible absorption peak (570 nm) exhibited by our Au–TiO_2 nanofibrous hybrid indicates that the LSPR absorption band of Au is red-shifted when Au nanoparticles are coupled with TiO_2. Earlier studies have reported that the LSPRs of Au nanoparticles are highly sensitive to the refractive index of the surrounding medium, where an increase in the local refractive index leads to a red-shift in the LSPR absorption peak (Mayer and Hafner, 2011; Huang et al., 2015). Thus, the red-shifted LSPR absorption band of Au in our hybrid nanofibers can be explained by the high refractive index of the TiO_2 matrix that hosts the embedded Au nanoparticles.

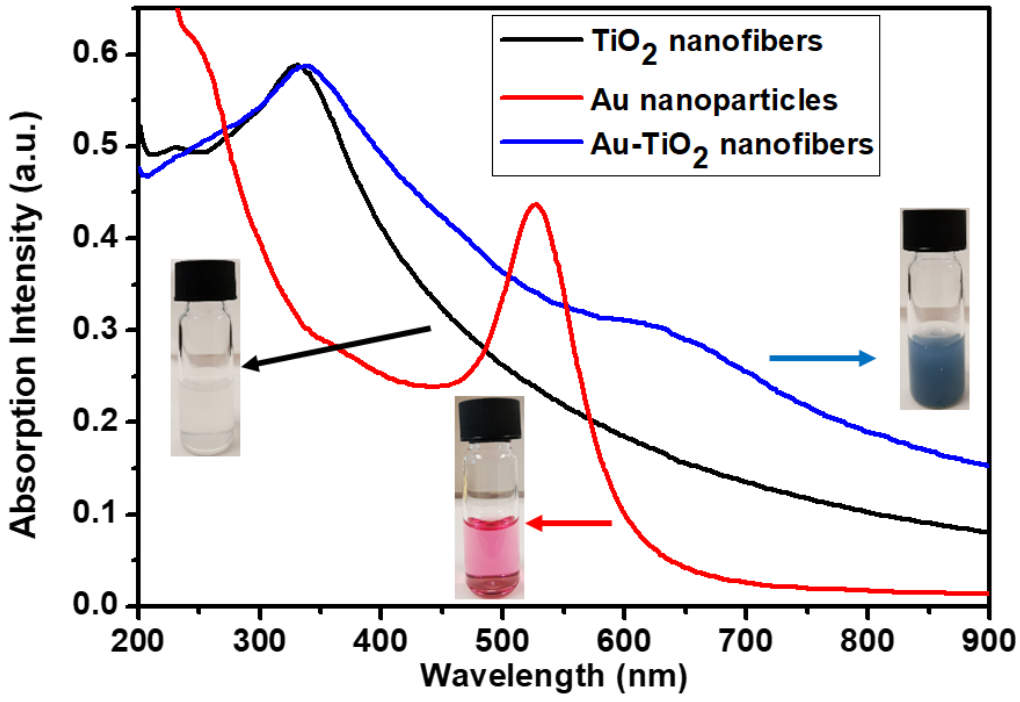

Fig. 4. UV-Vis absorption spectra of the pristine TiO_2 nanofibers (black), 5-nm Au nanoparticles (red) and Au-embedded TiO_2 nanofibers (blue). Insets show the photographs of aqueous dispersions of the three samples.

The strong absorption exhibited by the Au–TiO_2 nanofibrous hybrid in a wide spectral range that extends from the UV to the visible region makes it an attractive candidate for solar-driven photocatalysis. This has motivated us to investigate their potential as a solar-activated photocatalyst for the degradation of organic dyes, particularly RhB and MB. Fig. 5 shows the results of our photocatalytic dye degradation experiments. The data obtained for pristine TiO_2 nanofibers are also shown for comparison. For RhB degradation, the decrease in the dye concentration over time was monitored by measuring the absorbance of the characteristic RhB absorption peak at 553 nm (Fig. 5a-c). After 1 h of illumination using a solar simulator, 81% of the RhB dye in solution were degraded in the presence of the Au–TiO_2 nanofibers. When the illumination time was prolonged to 3 h, the percentage of dye degraded practically reached 100%, implying that the composite nanofibers are capable of completely degrading RhB under solar light with 3 h of illumination time. The corresponding change in color of the RhB solution can be seen in the inset of Fig. 5b. The intense pink color of the initial RhB solution became colorless after 3 h of continuous solar-light irradiation. The complete decolorization of the pink RhB solution signifies that none of the dye remains in the final solution. In the case of the pristine TiO_2 nanofibers, only 56% of RhB has been degraded after 3 h of solar-light irradiation under the same conditions. Thus, the pink color of the RhB solution is still evident even after 3 h of illumination time as seen in the inset of Fig. 5a. These results indicate that the TiO_2 nanofibers with embedded

Au nanoparticles are more effective as solar-light-responsive photocatalysts than the unmodified TiO_2 nanofibers.

A similar outcome was observed when the photocatalytic dye degradation experiments were performed using MB as the organic dye. For MB, the extent of degradation over time was monitored by taking the absorbance at 663 nm (Fig. 5d-f). After 3 h of solar-light illumination, 88% of MB in solution were degraded in the presence of the Au–TiO_2 nanofibers whereas only 67% were degraded by the pristine TiO_2 nanofibers. The photographs of the corresponding solutions show that the blue color of the initial MB solution turned substantially lighter after 3 h of illumination when degraded using the Au–TiO_2 nanofibers (inset in Fig. 5 e). By contrast, the characteristic blue color of MB is still very obvious in the final solution when pristine TiO_2 nanofibers were used. Again, this shows that the embedded Au nanoparticles are capable of boosting the photocatalytic performance of TiO_2.

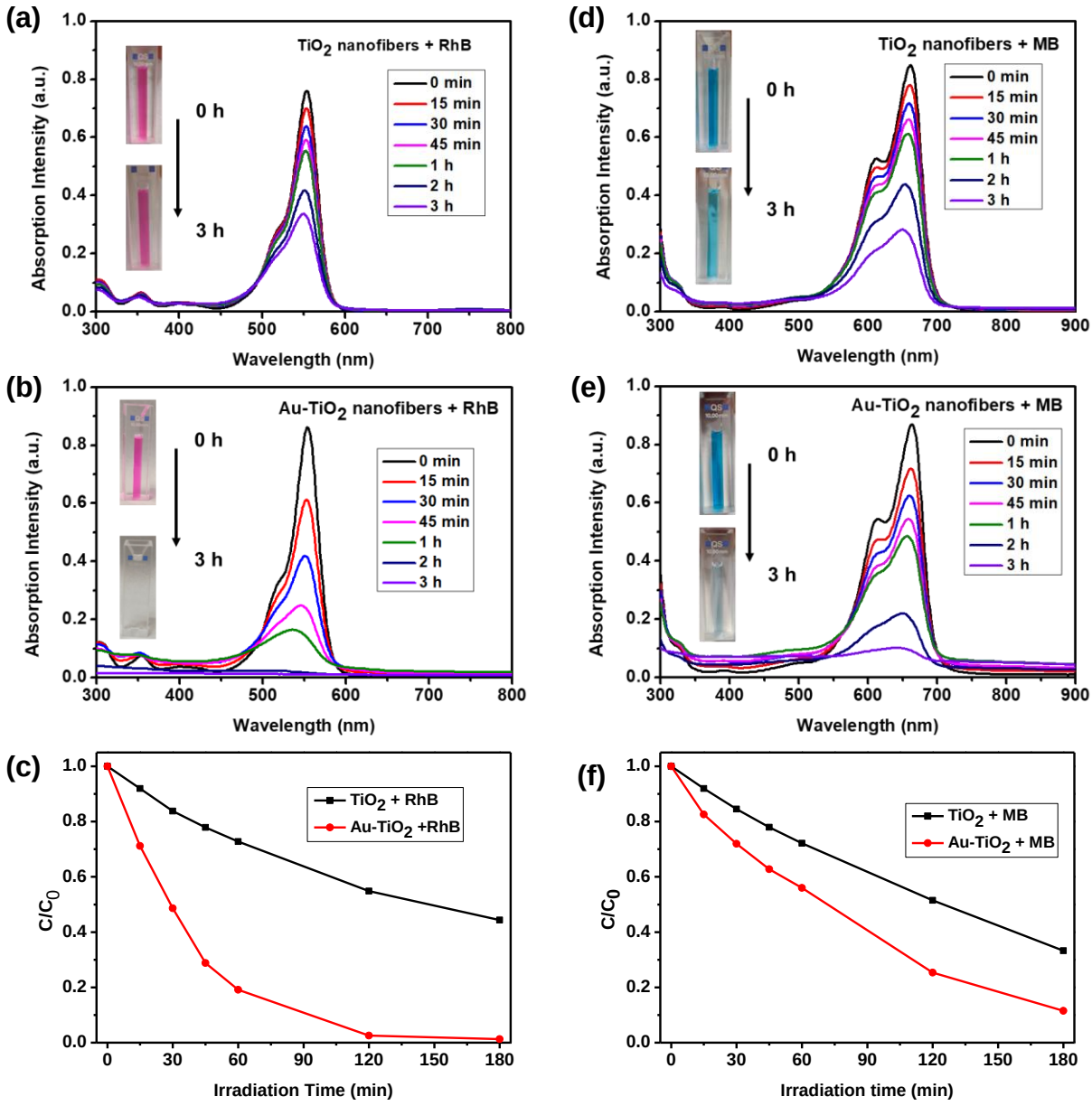

Fig. 5. Comparison of the photocatalytic performance of the pristine TiO_2 nanofibers and the Au–TiO_2 nanofibers in the photodegradation of (a-c) RhB and (d-f) MB under solar-light illumination. The inset photographs in (a,b) and (d,e) show the color change observed over time upon solar simulator irradiation of the pink RhB solution and blue MB solution in the presence of pristine TiO_2 nanofibers and Au–TiO_2 nanofibers.

The embedded Au nanoparticles in the composite nanofibers redresses the intrinsic limitations of pristine TiO_2, which is responsive only to UV light and exhibits rapid electron–hole recombination rate. Previous studies have explained the enhancement effect of plasmonic noble metals like Au on the photocatalytic behavior of TiO_2 through several proposed mechanisms (Bumajdad and Madkour, 2014). The mechanisms that are often cited are based on plasmon-enhanced photocatalysis, which is centered on the LSPR-induced visible-light absorption of Au nanoparticles (Linic et al., 2011). One example of such mechanisms involves a charge injection process, where the plasmon-induced photoexcitation of Au nanoparticles generates electron–hole pairs, of which the electrons are injected into the conduction band of TiO_2 (Yang et al., 2016). The separated charge carriers can then participate in redox reactions that drive the dye decomposition process. This mechanism is not favorable in composites with large Au nanoparticles (> 10 nm) due to the short mean free path of electrons in metals (Amrollahi et al., 2014). Another plasmon-related mechanism is based on the strong localization of electromagnetic fields at the Au–TiO_2 interface, which enhances the optical absorption of TiO_2 (Seh et al., 2012). In this case, the enhancement effect is more prominent in composites with large Au nanoparticles owing to their stronger plasmonic near-fields. We believe that both of these mechanisms contribute to the observed enhancement effect in our Au–TiO_2 nanofibers, with the first mechanism being the primary contributor considering the small size of the Au nanoparticles (ca. 5 nm) in our composite nanofibers. Aside from the plasmon-mediated enhancement mechanisms, which are driven by visible-light illumination, a UV-light-activated charge separation mechanism is also possible since we used a solar simulator that provides both UV and visible photons. The UV photons are absorbed by TiO_2 and the photogenerated electrons migrate from the conduction band of TiO_2 to Au due to

its lower Fermi energy level (Bumajdad et al., 2014). Thus, the presence of Au promotes charge separation, which leads to enhancement of photocatalytic activity.

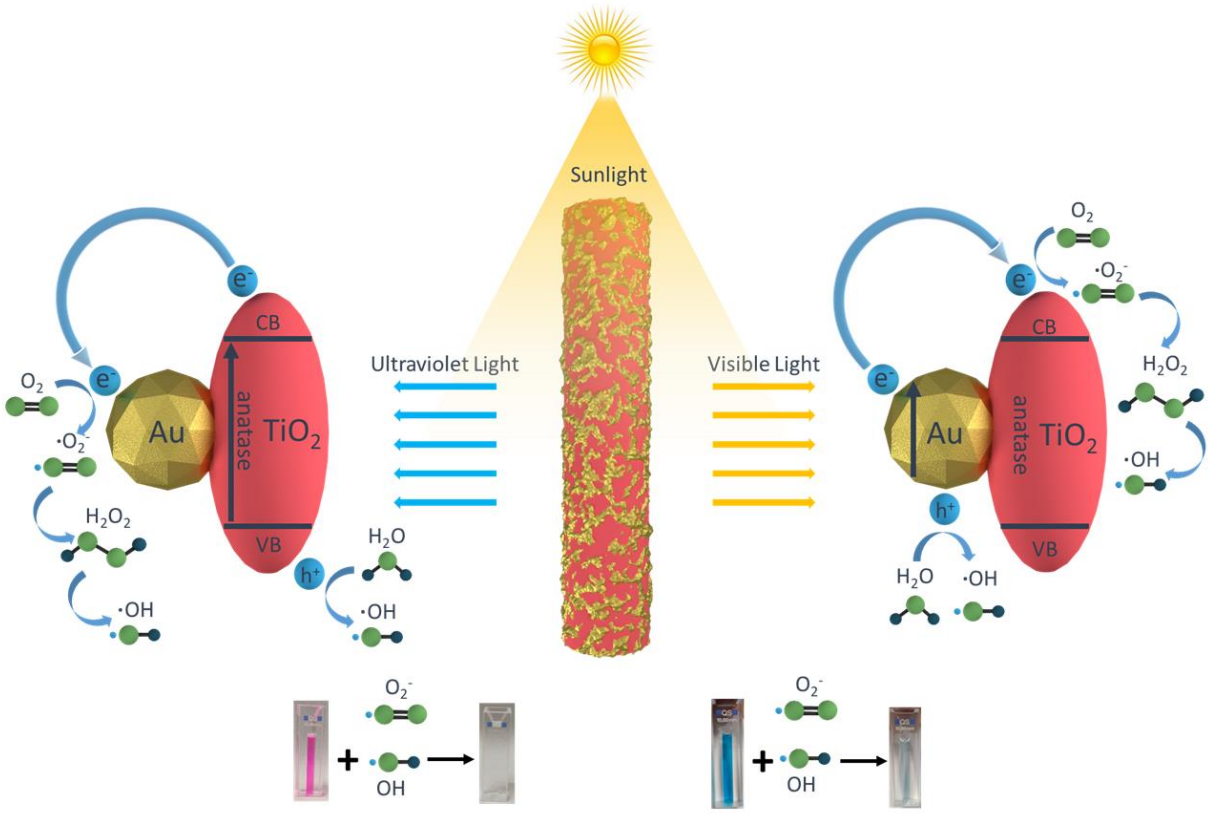

Fig. 6. Schematic illustration of the mechanisms that operate during solar-driven photocatalytic degradation of organic dye pollutants using Au–TiO_2 nanofibrous hybrid as a photocatalyst.

Fig. 6 provides a schematic illustration that summarizes the two charge separation mechanisms that are key contributors to the enhancement of the photocatalytic dye degradation activity of the Au–TiO_2 nanofibrous hybrid. Upon sunlight irradiation, both UV and visible light can lead to generation of electrons and holes. UV light is absorbed by TiO_2, and the excited electrons in the conduction band migrate to the neighboring Au nanoparticles, leading to effective charge separation at the heterojunction of the Au–TiO_2 hybrid. Meanwhile, visible light is absorbed by

the plasmonic Au nanoparticles, and the excited electrons are injected into the conduction band of TiO_2. This also results in charge separation. Once the photogenerated electrons and holes are effectively separated, they are free to participate in redox reactions. In photocatalytic degradation of organic dyes in aqueous media, the reaction generally proceeds as follows. The free electrons reduce dissolved O_2 to form anionic superoxide radicals ($\bullet O_2^-$), while the free holes oxidize H_2O to produce hydroxyl radicals (•OH) (Ajmal et al., 2014). These reactions are shown in Eq. 1 and 2. The superoxide radical can get protonated to form hydroperoxyl radical (HOO•), and then H_2O_2, which further dissociates into hydroxyl radicals (Eq. 3 to 5). The generated radicals subsequently attack organic dye pollutants and decompose them into smaller and less harmful compounds (Eq. 6 and 7). Note that during the degradation process, the conjugated chromophore of the dyes is destroyed. Since the chromophore gives the dyes their distinct color, the degradation products are colorless. Thus, when 100% degradation is achieved, the dye solution becomes completely decolorized.

$$e^- + O_2 \rightarrow \bullet O_2^- \quad (1)$$

$$h^+ + H_2O \rightarrow \bullet OH + H^+ \quad (2)$$

$$\bullet O_2^- + H^+ \rightarrow HOO\bullet \quad (3)$$

$$HOO\bullet \rightarrow H_2O_2 + O_2 \quad (4)$$

$$H_2O_2 + \rightarrow 2\ \bullet OH \quad (5)$$

$$\text{Dye} + \bullet O^{2-} \rightarrow \text{degradation products} \quad (6)$$

$$\text{Dye} + \bullet OH \rightarrow \text{degradation products} \quad (7)$$

One of the most important features that defines a good photocatalyst is its reusability. We have recovered the Au–TiO_2 nanofibers that were used for the RhB degradation experiment and

subjected them to another cycle of use. Fig. 7a shows that the recycled Au–TiO_2 nanofibers were again able to completely degrade RhB after 3 h of solar-light illumination. The degradation rate for the 2nd cycle is the same as that observed for the 1st cycle, as seen in the graph in Fig. 7b. The ability of the recovered photocatalyst to retain its photocatalytic efficiency is a clear indication that the Au–TiO_2 nanofibers are stable and recyclable, which are necessary for practical applications. The TEM images (Fig. S1, Supplemental) of the Au–TiO_2 nanofibers that were taken after reuse showed no apparent changes in the composite configuration and morphology, which further confirms the stability of the hybrid photocatalyst.

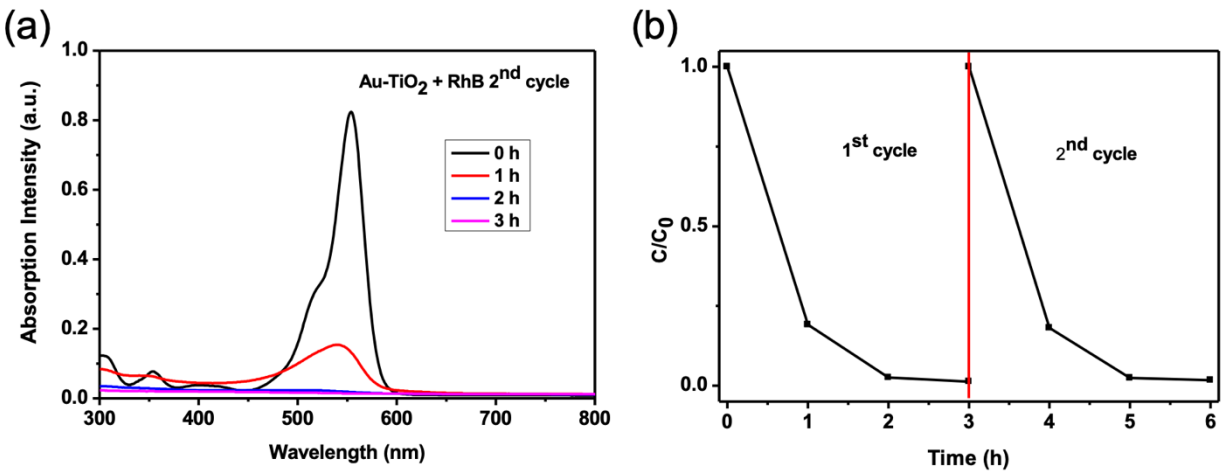

Fig. 7. (a) Photocatalytic degradation of RhB using recycled Au–TiO_2 nanofibers under solar-light irradiation. (b) Photocatalytic RhB degradation rate of Au–TiO_2 nanofibers in the 1st and 2nd cycle of use.

4. Conclusions

Solar-driven photocatalytic dye degradation offers an effective means of clearing industrial wastewater of hazardous dye pollutants prior to its release into the environment. This work reported the fabrication of a solar-light-responsive composite photocatalyst, which is based on electrospun TiO_2 nanofibers that contain embedded Au nanoparticles. The presence of Au nanoparticles is crucial to the enhancement of the photocatalytic activity of pristine TiO_2, which is responsive only to UV light and exhibits fast charge recombination rate. The advantages of coupling TiO_2 with Au is manifested by the superior photocatalytic performance displayed by the Au–TiO_2 nanofibers relative to the pristine TiO_2 nanofibers in the decomposition of RhB and MB dyes under solar simulator irradiation. The Au–TiO_2 nanofibers were also shown to be stable and recyclable, which are properties that are highly desired in a photocatalyst.

Acknowledgments

M. D. Regulacio acknowledges funding support from the National Sciences Research Institute (NSRI, Project CHE-20-1-02) of UP Diliman.

Appendix A. Supplementary data

Supplementary data to this article is available online.

References

Ajmal, A., Majeed, I., Malik, R.N., Idriss, H., Nadeem, M.A., 2014. Principles and mechanisms of photocatalytic dye degradation on TiO 2 based photocatalysts: a comparative overview. RSC Adv. 4, 37003-37026.

Al-Hamdi, A.M., Rinner, U., Sillanpää, M., 2017. Tin dioxide as a photocatalyst for water treatment: a review. Process Safety and Environmental Protection 107, 190-205.

Al-Mamun, M., Kader, S., Islam, M., Khan, M., 2019. Photocatalytic activity improvement and application of UV-TiO2 photocatalysis in textile wastewater treatment: a review. J. Environ. Chem. Eng. 7, 103248.
Amrollahi, R., Hamdy, M.S., Mul, G., 2014. Understanding promotion of photocatalytic activity of TiO2 by Au nanoparticles. J. Catal. 319, 194-199.
Berradi, M., Hsissou, R., Khudhair, M., Assouag, M., Cherkaoui, O., El Bachiri, A., El Harfi, A., 2019. Textile finishing dyes and their impact on aquatic environs. Heliyon 5, e02711.
Bumajdad, A., Madkour, M., 2014. Understanding the superior photocatalytic activity of noble metals modified titania under UV and visible light irradiation. Phys. Chem. Chem. Phys. 16, 7146-7158.
Bumajdad, A., Madkour, M., Abdel-Moneam, Y., El-Kemary, M., 2014. Nanostructured mesoporous Au/TiO 2 for photocatalytic degradation of a textile dye: the effect of size similarity of the deposited Au with that of TiO 2 pores. J. Mater. Sci. 49, 1743-1754.
Chan, S.H.S., Yeong Wu, T., Juan, J.C., Teh, C.Y., 2011. Recent developments of metal oxide semiconductors as photocatalysts in advanced oxidation processes (AOPs) for treatment of dye waste‐water. Journal of Chemical Technology & Biotechnology 86, 1130-1158.
Cossich, E., Bergamasco, R., De Amorim, M.P., Martins, P., Marques, J., Tavares, C.J., Lanceros-Méndez, S., Sencadas, V., 2015. Development of electrospun photocatalytic TiO2-polyamide-12 nanocomposites. Mater. Chem. Phys. 164, 91-97.
Djurišić, A.B., Leung, Y.H., Ng, A.M.C., 2014. Strategies for improving the efficiency of semiconductor metal oxide photocatalysis. Mater. Horiz. 1, 400-410.
Duan, Z., Huang, Y., Zhang, D., Chen, S., 2019. Electrospinning fabricating Au/TiO 2 network-like nanofibers as visible light activated photocatalyst. Sci. Rep. 9, 1-8.
Gautam, A., Kshirsagar, A., Biswas, R., Banerjee, S., Khanna, P.K., 2016. Photodegradation of organic dyes based on anatase and rutile TiO 2 nanoparticles. RSC Adv. 6, 2746-2759.
Gopinath, K.P., Madhav, N.V., Krishnan, A., Malolan, R., Rangarajan, G., 2020. Present applications of titanium dioxide for the photocatalytic removal of pollutants from water: A review. J. Environ. Manage. 270, 110906.
He, K., Chen, G., Zeng, G., Chen, A., Huang, Z., Shi, J., Huang, T., Peng, M., Hu, L., 2018. Three-dimensional graphene supported catalysts for organic dyes degradation. Applied Catalysis B: Environmental 228, 19-28.
Hoffmann, M.R., Martin, S.T., Choi, W., Bahnemann, D.W., 1995. Environmental applications of semiconductor photocatalysis. Chem. Rev. 95, 69-96.
Hu, M., Chen, J., Li, Z.-Y., Au, L., Hartland, G.V., Li, X., Marquez, M., Xia, Y., 2006. Gold nanostructures: engineering their plasmonic properties for biomedical applications. Chem. Soc. Rev. 35, 1084-1094.
Huang, M.H., Rej, S., Chiu, C.Y., 2015. Facet‐Dependent Optical Properties Revealed through Investigation of Polyhedral Au–Cu2O and Bimetallic Core–Shell Nanocrystals. Small 11, 2716-2726.
Khalid, N., Majid, A., Tahir, M.B., Niaz, N., Khalid, S., 2017. Carbonaceous-TiO2 nanomaterials for photocatalytic degradation of pollutants: A review. Ceram. Int. 43, 14552-14571.
Kochkina, N.E., Agafonov, A.V., Vinogradov, A.V., Karasev, N.S., Ovchinnikov, N.L., Butman, M.F., 2017. Photocatalytic activity of biomorphic TiO2 fibers obtained by ultrasound-assisted impregnation of cellulose with titanium polyhydroxocomplexes. ACS Sustain. Chem. Eng. 5, 5148-5155.
Kumar, L., Singh, S., Horechyy, A., Formanek, P., Hübner, R., Albrecht, V., Weißpflog, J., Schwarz, S., Puneet, P., Nandan, B., 2020. Hollow Au@ TiO 2 porous electrospun nanofibers for catalytic applications. RSC Adv. 10, 6592-6602.
Lellis, B., Fávaro-Polonio, C.Z., Pamphile, J.A., Polonio, J.C., 2019. Effects of textile dyes on health and the environment and bioremediation potential of living organisms. Biotechnology Research and Innovation 3, 275-290.
Li, D., Xia, Y., 2003. Fabrication of titania nanofibers by electrospinning. Nano Lett. 3, 555-560.

Li, J., Zeng, H.C., 2005. Size tuning, functionalization, and reactivation of Au in TiO2 nanoreactors. Angew. Chem. Int. Ed. 44, 4342-4345.
Ligon, C., Latimer, K., Hood, Z.D., Pitigala, S., Gilroy, K.D., Senevirathne, K., 2018. Electrospun metal and metal alloy decorated TiO 2 nanofiber photocatalysts for hydrogen generation. RSC Adv. 8, 32865-32876.
Linic, S., Christopher, P., Ingram, D.B., 2011. Plasmonic-metal nanostructures for efficient conversion of solar to chemical energy. Nat. Mater. 10, 911-921.
Ma, Y., Wang, X., Jia, Y., Chen, X., Han, H., Li, C., 2014. Titanium dioxide-based nanomaterials for photocatalytic fuel generations. Chem. Rev. 114, 9987-10043.
Mayer, K.M., Hafner, J.H., 2011. Localized surface plasmon resonance sensors. Chem. Rev. 111, 3828-3857.
Nam, Y., Lim, J.H., Ko, K.C., Lee, J.Y., 2019. Photocatalytic activity of TiO 2 nanoparticles: a theoretical aspect. J. Mater. Chem. A 7, 13833-13859.
Roongraung, K., Chuangchote, S., Laosiripojana, N., Sagawa, T., 2020. Electrospun Ag-TiO2 Nanofibers for Photocatalytic Glucose Conversion to High-Value Chemicals. ACS omega 5, 5862-5872.
Seh, Z.W., Liu, S., Low, M., Zhang, S.Y., Liu, Z., Mlayah, A., Han, M.Y., 2012. Janus Au‐TiO2 photocatalysts with strong localization of plasmonic near‐fields for efficient visible‐light hydrogen generation. Adv. Mater. 24, 2310-2314.
Seh, Z.W., Liu, S., Zhang, S.Y., Bharathi, M., Ramanarayan, H., Low, M., Shah, K.W., Zhang, Y.W., Han, M.Y., 2011. Anisotropic growth of titania onto various gold nanostructures: synthesis, theoretical understanding, and optimization for catalysis. Angew. Chem. 123, 10322-10325.
Someswararao, M., Dubey, R., Subbarao, P., Singh, S., 2018. Electrospinning process parameters dependent investigation of TiO2 nanofibers. Results in Physics 11, 223-231.
Soo, J.Z., Lee, K.M., Ang, B.C., Ong, B.H., 2019. Optimal Electrospun TiO2 Nanofiber Photocatalytic Performance via Synergistic Morphology and Particle Crystallinity with Anatase/Rutile Phase Tuning. physica status solidi (a) 216, 1900066.
Thuong, H.T.T., Kim, C.T.T., Quang, L.N., Kosslick, H., 2019. Highly active brookite TiO2-assisted photocatalytic degradation of dyes under the simulated solar− UVA radiation. Progress in Natural Science: Materials International 29, 641-647.
Yang, B., He, D., Wang, W., Zhuo, Z., Wang, Y., 2016. Gold-plasmon enhanced photocatalytic performance of anatase titania nanotubes under visible-light irradiation. Mater. Res. Bull. 74, 278-283.

Graphical Abstract